

## On the performance of a dual-beam polarimeter at Kodaikanal Tower Telescope

K. Nagaraju\*, K. Sankarasubramanian†, K. E. Rangarajan, K. B. Ramesh, Jagdev Singh, P. Devendran and Hariharan

*Indian Institute of Astrophysics, Bangalore 560 034, India*

*†Space Astronomy and Instrumentation Division, ISRO Satellite center, Bangalore 560094, India*

Received 12 April 2008; accepted 26 August 2008

**Abstract.** Calibration and characterization of a dual-beam polarimeter installed at Kodaikanal Tower Telescope (KTT) for spectropolarimetric observations are presented in this paper. It was found that a slit width of  $48 \mu$  is optimum for the spectrograph setup at KTT and corresponding spectral resolution is  $32.47 \text{ m}\text{\AA}$ . It was demonstrated that the precision in polarization measurement can be achieved better than 0.1 % by increasing the exposure time. However, the polarimetric calibration accuracy is limited to 0.35 % for Stokes  $Q$  and  $U$  parameters and 0.2 % for Stokes  $V$  parameter, mainly due to the uncertainty in the retardance of the calibration retarder. A comparison of the magnetic field measurement between the Solar Optical Telescope (SOT) onboard *Hinode* and KTT for an active region was made and a good match was found after spatial smearing of *Hinode*/SOT measurements by  $5.12''$ .

*Keywords :* Instrumentation : polarimeter

### 1. Introduction

Measurement of magnetic field on the Sun and its interpretation is important to understand the dynamics that take place in the solar atmosphere and beneath. It is known that spectropolarimetry is a powerful observational tool for the accurate measurement of the magnetic field. In addition to the magnetic field, several other atmospheric parameters such as temperature, density, velocity, etc., can be derived using spectropolarimetric

---

\*e-mail:nagaraj@iiap.res.in

data. For the purpose of carrying out spectropolarimetric observations, a dual-beam polarimeter was installed at KTT (Nagaraju et al. (2007); paper I).

Accuracy and precision in the polarization measurements determine the accuracy in the derived magnetic field. Apart from this, accurate knowledge about the characteristics of the instrument is important for reliable inference of the physical parameters through spectropolarimetry. Towards this goal, a few experiments were carried out to characterize the spectropolarimetric setup at KTT. Polarimetric calibration data were obtained almost on a daily basis during the observations. All the calibration procedures are based on basic principles of physics. However, a comparison of the measurements using this instrument with those obtained from other instruments help in establishing reliability of the measurements and collaborative observations can be undertaken along with other instruments for better understanding of solar activities. Here, we compare the magnetic field measured at KTT with near simultaneous *Hinode*/SOT measurements.

## 2. Spectropolarimetric observations

The instrumental setup for simultaneous imaging and spectropolarimetry at KTT is as shown in Fig. 1. Further details on the optical setup are discussed in the following sections.

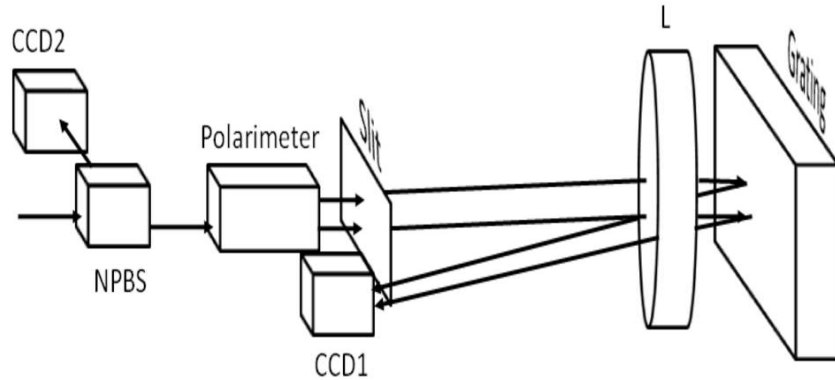


**Figure 1.** Schematic diagram of the spectropolarimetric observing setup at KTT. The terms in the diagram are L - Collimator, NPBS - Non-Polarizing Beam Splitter, CCD1 and CCD2 - charge coupled devices for recording spectrum and images, respectively.

### 2.1 Polarimeter setup

The polarimeter consists of a polarizing beam displacer (PBD) and two retarders (quarter and half waveplates at 630 nm), marked as R1 and R2 in Fig. 2. The retarders mounted on

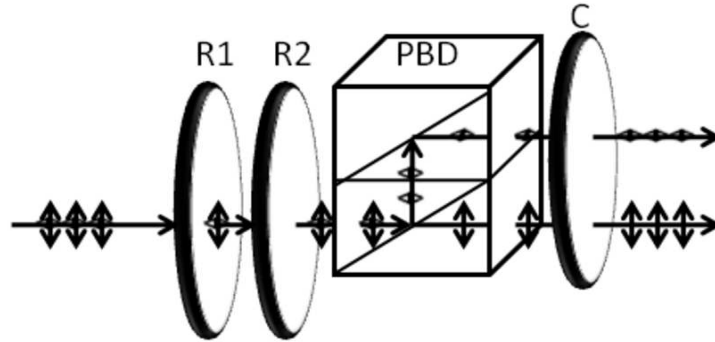


**Figure 2.** Schematic diagram of a dual-beam polarimeter setup at KTT. The terms in this figure are R1, R2 - polarization modulators, PBD - Polarizing Beam Displacer and C - polarization compensator.

separate rotating stages are placed in front of the PBD with quarter waveplate followed by half waveplate. The entire setup of the polarimeter is placed in front of the spectrograph slit (Fig. 1). Two beams coming out of the polarimeter are orthogonally linearly polarized with the direct beam polarized in the direction of the slit and the vertically displaced beam polarized in the perpendicular direction. The clear aperture of the PBD is 10 mm in the slit direction which restricts the field-of-view (FOV) to  $55''$  on the Sun for a given slit position. A linear polarizer is placed behind the PBD, marked as C in Fig. 2, with its optic axis at  $45^\circ$  with respect to the spectrograph slit to compensate for the differential response of the spectrograph grating to the orthogonal states of linear polarization. The orthogonally polarized beams are recorded using a CCD camera (marked as CCD1 in Fig. 1) placed just below the spectrograph slit after getting dispersed from the grating.

## 2.2 Imaging setup

To perform simultaneous imaging of the region-of-interest (ROI) in continuum a non-polarizing beam splitter (NPBS) is used to split the beam before entering the polarimeter such that the reflected beam forms an image of the ROI on a CCD (marked as CCD2 in Fig. 1) and the transmitted beam is used for spectropolarimetric measurements. The NPBS is made of BK7 glass with a transmission ratio of 50%. The clear aperture of the beam splitter is  $126''$ . At present the images are taken in continuum through a broadband filter (bandwidth of  $800 \text{ \AA}$ ). This imaging facility can be used more effectively with narrow band filters centered around the spectral lines originating in the chromosphere (for e.g.,  $H\alpha$ , Ca or Na lines). This will help in positioning the spectrograph slit on the chromospheric structures, which are not seen in the continuum images.

To identify the corresponding slit position on the image, a circular aperture was introduced in front of the NPBS. This aperture produces circular images on the slit as

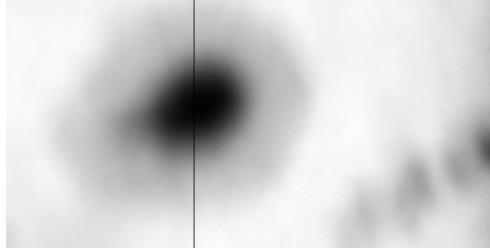


**Figure 3.** Image of an active region (NOAA0940) in the broad wavelength band taken at KTT on February 1, 2007 with an artificial slit position marked on it.

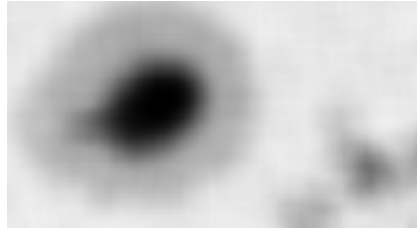


**Figure 4.** Raster image of the active region (NOAA0940) in the continuum wavelength close to 6300 Å observed by *Hinode*/SOT on February 1, 2007. The image is smoothed by  $16 \times 16$  pixels to compare with the image obtained at KTT.

well as on CCD2. The position of this aperture was adjusted such that the centre of the circular image passes through the slit. Hence the pixel column at the centre of this circular image recorded by CCD2 would roughly correspond to the slit position. Although this is a crude way of identifying the slit position on the image, the mislocation of the slit is well within the resolution limit. This was confirmed by comparing the intensity variation across the raster images of spectropolarimetric observations. Since the magnification of the image by the spectrograph is almost equal to one, and no other optics except the filters are used for imaging, the image scales in the images and spectrum along the slit direction are same. A sample image of an active region is shown in Fig. 3 with an artificial slit marked on it. For comparison a raster image of the same active region obtained in the continuum close to 630 nm of the spectropolarimetric observations by *Hinode*/SOT is shown in Fig. 4. *Hinode* image is spatially smeared by  $5.12'' \times 5.12''$  in order to roughly get one-to-one correspondence between the images. Further, this same active region is considered in section 4.3 for comparing the magnetic field measurements between KTT and *Hinode*/SOT. Identification of the slit could be done in a more systematic way by having a re-imaging facility in which case a reference hair line could be placed in the image plane of the re-imaging system and the slit location could be identified more accurately on the images. This is being planned as a future improvement.

There is a disadvantage with the currently used NPBS as its transmission ratio is

50% and hence the photons available for spectropolarimetry are reduced at least by 50%. On the other hand the available photons are in excess for wide band imaging. However, a NPBS with an appropriate transmission ratio shall be selected depending on the narrow band filters to be used for imaging.

### 2.3 Observations

Scanning of the ROI on the Sun is usually done by moving the Sun's image in an East-West direction in steps of  $\approx 2''$  during good/moderate seeing conditions and  $\approx 5''$  during bad seeing conditions. Images of the ROI in broad wavelength band are recorded for each stage of polarization modulation.

## 3. Spectropolarimetric data reduction

### 3.1 Flat fielding

The beam swapping technique (c.f., Donati et al. 1990) which is inbuilt in the modulation/demodulation scheme presented in paper I helps in alleviating the gain table errors in the polarization data without the need for flat fielding. However, for total intensity, the flat fielding correction is essential. For the flat fielding, spectral images were recorded (without changing the observing setup) by moving the solar image randomly over the slit during the exposure. The quiet Sun region close to disk centre, which is free from any visible activity, is normally chosen for flat fielding. The random movement of the Sun's image smears out the solar structures like granules. This way, we can get a nearly uniform light along the slit, but the spectral features remain unchanged. Spectral features are removed by dividing each spectral profile by an average profile taken along the slit and the resultant pixel values are the gain table factors. Before this, the curvatures in the spectral features along the slit need to be corrected. Finding out the curvature and correcting them is done as follows. The two spectral images corresponding to vertically and horizontally polarized beams are considered separately to calculate the spectral curvatures along the slit. A reference profile was considered at the centre of each beam and then the shifts of other profiles with respect to the reference profile are obtained using a correlation technique. The shifted values are then fitted to a linear curve and these fitted values are used for aligning the spectral lines using a Fourier shift algorithm. Further, the gain table difference between the two beams is corrected using the ratio between the maximum pixel value of the corresponding beam. The resultant spectral images without spectral features are flat frames. Separate flat frames are obtained for each stage of polarization modulation step. Respective flat frames are used to correct for gain table variation for the observed spectral images for a given stage of modulation before combining the eight measurements to derive the Stokes parameters. This method of flat fielding

helps in reducing the polarization dependent fringes to some extent (More details can be found in Beck et al. 2005).

### 3.2 Polarimeter response

Calibration data are obtained almost on daily basis during the observations using the calibration unit described in paper I. Using the calibration data and the input Stokes parameters, constructed out of the known properties of the calibration optics (c.f., paper I), the response matrix of the polarimeter is obtained. The measured Stokes parameters are then corrected for the polarimeter response. The calibration accuracy of Stokes  $Q$  and  $U$  are limited to 0.35% and 0.2% for Stokes  $V$  parameter. The calibration error is mainly caused due to the uncertainty in the retardance value of the calibration unit retarder (see paper I for more details).

### 3.3 Telescope induced cross-talks

Oblique reflections of the sunlight from the coelostat mirrors of KTT modify the polarization state of input light resulting in cross-talk among Stokes parameters. This is corrected using a telescope model developed by Balasubramaniam, Venkatakrishnan & Bhattacharya (1985) and Sankarasubramanian (2000) for KTT. Since the refractive index values used in the model were taken from the literature (c.f., Walter 1978), which may well be different from the actual values, there remains a cross-talk among Stokes parameters (see the dash-dotted curves in Fig. 5). This residual cross-talk is removed using a statistical method described in Sanchez Almeida & Lites (1992) and Schlichenmaier & Collados (2002) (the solid curves in Fig. 5). Stepwise correction of instrumental polarization is demonstrated in Fig. 5. For this purpose Stokes profiles of Fe I line (6569 Å) observed in the penumbral region of the active region NOAA0940 (c.f., Fig. 3) are shown in this figure. The top left and right panels show the Stokes  $I$  and  $Q/I$  profiles and the bottom left and right panels show Stokes  $U/I$  and  $V/I$  profiles, respectively.

## 4. Characterization of the spectropolarimeter at KTT

### 4.1 Experiment to study the spectral resolution of the spectrograph

An experiment was carried out to determine an optimum width for the spectrograph slit and measure the corresponding spectral resolution. A parallel beam of He-Ne laser was passed through the objective of the KTT so that the laser beam is focussed on to the spectrograph slit. For a given spectral order, the laser profiles were recorded by varying the slit width from 30-150  $\mu$  in steps of 10  $\mu$ . The observed laser profiles were fitted using a Gaussian function. A sample observed profile with the fitted Gaussian profile

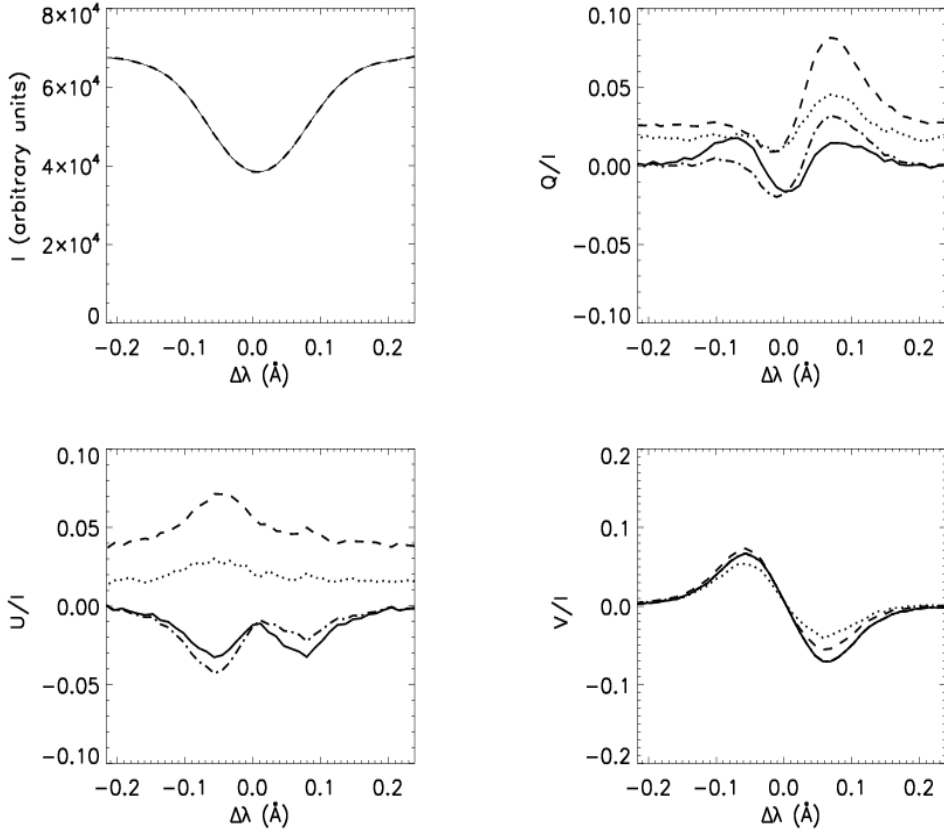


**Figure 5.** Demonstration of stepwise correction of Stokes profiles for instrumental polarization. The top left and right panels show Stokes  $I$  and  $Q/I$  profiles, the bottom left and right panels show Stokes  $U/I$  and  $V/I$  profiles, respectively. The dotted curves correspond to the observed Stokes profiles and the dashed curves correspond to the profiles after correcting for polarimeter response. The Stokes profiles after correcting for telescope induced cross-talk using a telescope model are shown as the dash-dotted curves. The solid curves correspond to the profiles after correcting for residual cross-talk among Stokes parameters using a statistical method.

overplotted on it (the solid curve) is shown in Fig. 6. The Full Width at Half Maximum (FWHM) of the laser profiles were calculated using the formula

$$FWHM = 2(\sqrt{2\ln 2})\sigma, \quad (1)$$

where  $\sigma$  is the width of the Gaussian function. The plot of FWHM versus the slit width is shown in Fig. 7. The solid lines in this figure are the linear fit to the FWHM values fitted separately for the set of values which are almost constant with respect to the slit width and the other set of FWHM values which increase monotonically with the slit width. The error bars are 3 times the fit error of the FWHM obtained through Gaussian fit of

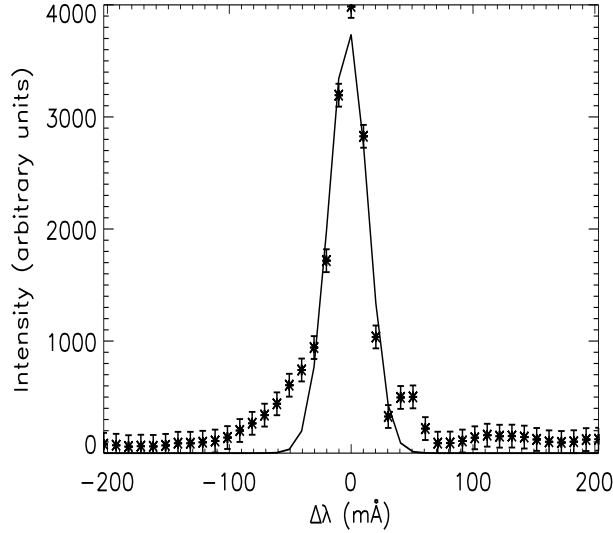


**Figure 6.** A sample laser profile recorded in the second order of spectrum for the slit width of  $50 \mu$ . The Gaussian profile fitted to this profile is overplotted on it (solid curve). The error bars shown in the plot are the photon noise associated with the intensity measurements.

the profiles. In Fig. 7 the FWHM does not change upto the slit width value of  $\approx 48 \mu$  after which it increases monotonically. Hence the optimum slit width for the Kodaikanal spectrograph setup was selected to  $48 \mu$  and the corresponding spectral resolution is  $32.47 \text{ m}\text{\AA}$  in the second order of spectrum.

## 4.2 Photon noise

Another simple experiment was performed in order to determine the noise in the measurement of the Stokes parameters and to study its behaviour as a function of exposure time. For a given exposure time, a set of eight spectral images were recorded by orientating the polarimeter retarders at the angles required for eight stage modulation scheme (paper I). These eight intensity measurements were combined according to the demodulation scheme explained in paper I to form Stokes spectral images. The above procedure was repeated for different exposure times varying from 200 to 2400 ms in steps of 200 ms. The standard deviations of Stokes parameters ( $\sigma_{IQUV}$ s) were calculated over 256 pixels at different wavelength points in the corresponding Stokes images, where  $\sigma_{IQUV}$  represent the noise in the corresponding Stokes parameters. A plot of  $\sigma_{IQUV}$  as a function of exposure time is shown in Fig. 8. The error bars are twice the rms values of  $\sigma_{IQUV}$  calculated at different wavelengths around  $6563 \text{ \AA}$ . Note that  $\sigma_{IQUV}$  closely follow the Poissonian statistics (the solid lines in the plots) implying that a better precision in the measurement of the Stokes parameters can be achieved by increasing the exposure time.

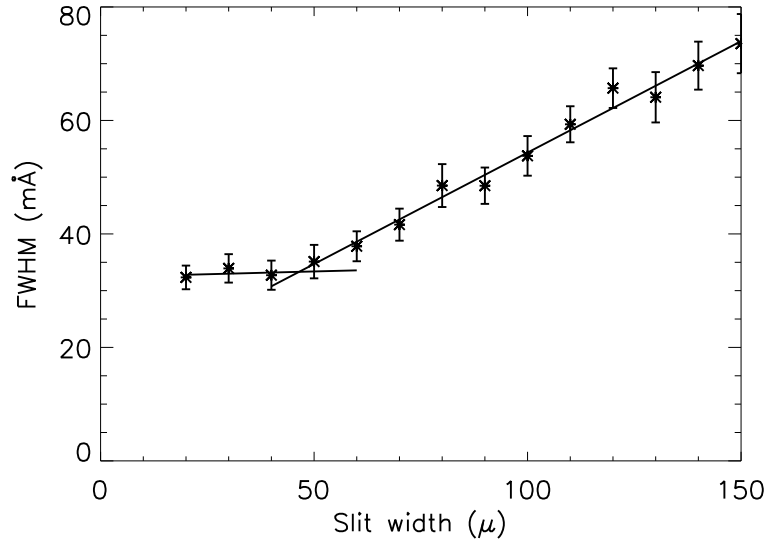


**Figure 7.** FWHM of He-Ne laser profile (asterisk symbol) as a function of the slit width. The error bars are 3 times the fit error of the FWHM when a Gaussian is fitted to the observed profile. The solid lines are the linear fit to the FWHM values fitted separately for the set of values which are almost constant with respect to the slit width and the other set of FWHM values which increase monotonically with the slit width.

For the exposure time of 2400 ms it was found that the polarimetric precision is better than 0.1%.

#### 4.3 Comparison of vector magnetic field of an active region measured at KTT with that of the *Hinode*/SOT

To compare the vector magnetic field measurements at KTT and *Hinode*/SOT at the photosphere, spectropolarimetric observations of an active region were analyzed. The active region considered was NOAA0940 located close to disk centre. The observations of the sunspot at KTT considered here are about five and half hours ahead of *Hinode*/SOT observations (c.f., Figs 3 and 4). Vector magnetic fields at the photosphere were obtained by inverting the Stokes profiles of Fe I line at 6569 Å for KTT data and Fe I line pair at 6300 Å for *Hinode*/SOT data under Milne-Eddington atmospheric model using the High Altitude Observatory inversion code.

For the comparison of the magnetic field measured by these two instruments, the image scales were matched using the respective plate scales of the imaging system. Further, the *Hinode*/SOT observations were smoothed by  $16 \times 16$  pixels (equivalent of  $5.12'' \times 5.12''$ ) to spatially match with the magnetic field strengths measured by KTT.

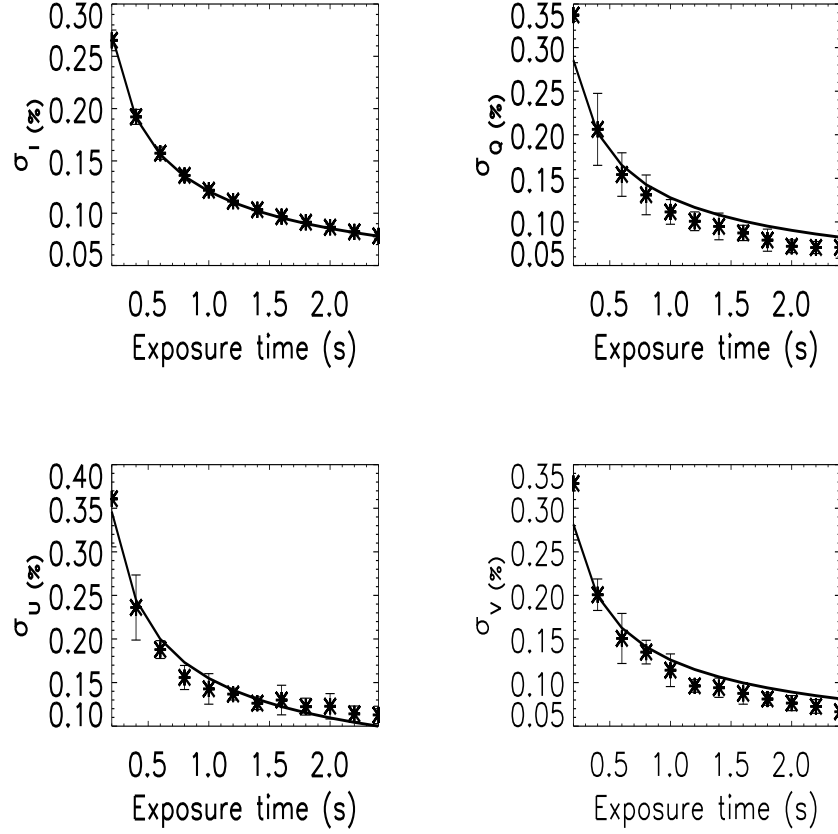


**Figure 8.** The rms noise of Stokes parameters ( $\sigma_{IQUV}$ ) as a function of exposure time. Error bars are 2 times the rms variation of  $\sigma_{IQUV}$  calculated at different wavelength points around 6563 Å.

Scatter plot of total field strength of KTT measurements and *Hinode* measurements is shown in Fig. 9. The solid line in the plot is a linear fit to the data points. The slope of this linear fit is 1.009. The spread in the data points may be due to the lack of exact one-to-one spatial correspondence which arises because of the poor sampling of the spectropolarimetric data at KTT during the sunspot scan. The step size used for scanning the sunspot was  $\approx 2''$ . This is also a limitation on producing a reasonable vector magnetic map of the ROI.

## 5. Summary

An optimum slit width of  $48 \mu$  was found for KTT spectrograph in the second order of diffraction corresponding to a spectral resolution of  $32.47 \text{ m}\text{\AA}$  at  $6328 \text{ \AA}$ . It was found

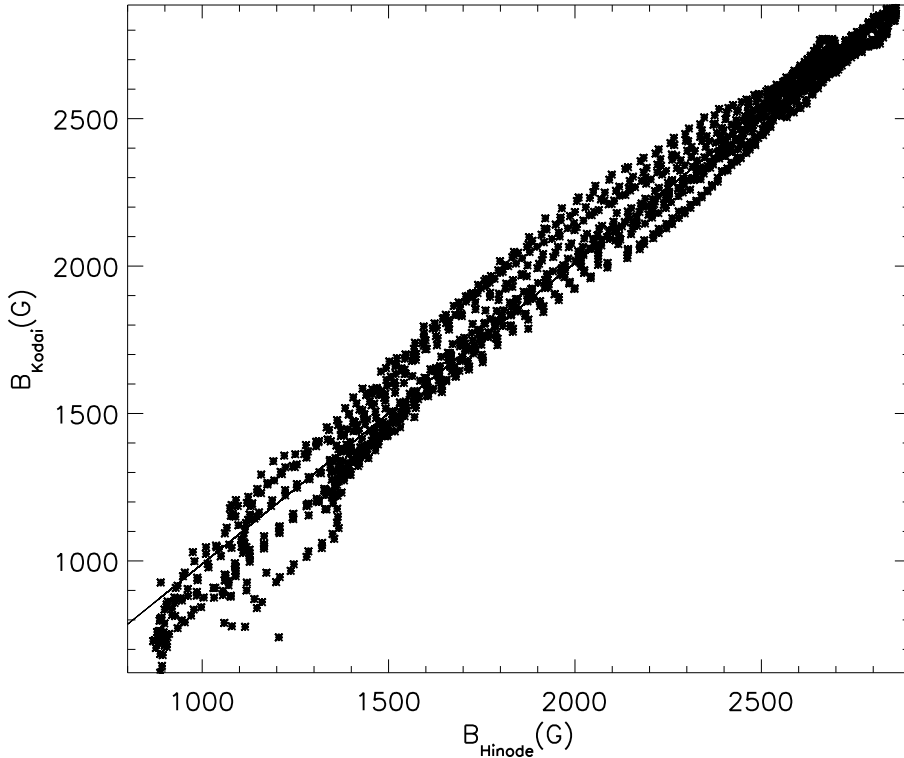


**Figure 9.** Scatter plot of magnetic field strengths measured at KTT and by *Hinode*/SOT. The sunspot considered for comparison was NOAA0940 which was located close to disk centre during observations. For the sake of brevity the error bars are not plotted. However, the errors in estimating the magnetic field are less than 50 G.

through another experiment that the noise in the polarization data is mostly limited by the photon noise and for the exposure time of 2.4 s the noise level is better than 0.1%. However the calibration accuracies of Stokes  $Q$  and  $U$  parameters are limited to 0.35% and Stokes  $V$  to 0.2% which could be improved by using a better calibrated retarder used for calibration purpose. The magnetic field strengths measured at KTT has a nearly one-to-one correspondence with that of the space based observations of *Hinode*/SOT after spatially smearing the *Hinode*/SOT measurements by  $5.12'' \times 5.12''$ .

## Acknowledgments

We would like to thank the referee for his useful suggestions for the improvement of the manuscript. Thanks to Mr. George for his help in setting up of the imaging system at KTT. *Hinode* is a Japanese mission developed and launched by ISAS/JAXA, with NAOJ

as domestic partner and NASA and STFC (UK) as international partners. It is operated by these agencies in co-operation with ESA and NSC (Norway).

### References

- Balasubramaniam, K. S., Venkatakrisnan, P., & Bhattacharya, J. C., 1985, *Sol. Phys.*, 99, 333  
Beck, C., Schmidt, W., Kentischer, T., & Elmore, D. F., 2005, *A&A*, 437, 1159  
Donati, J. F., Semel, M., Rees, D. E., Taylor, K., & Robinson, R. D., 1990, *A&A*, 232, L1  
Nagaraju, K., Ramesh, K. B., Sankarasubramanian, K., & Rangarajan, K. E., 2007, *BASI*, 35, 307  
Sanchez Almeida, J., & Lites, B. W., 1992, *ApJ*, 398, 359  
Sankarasubramanian, K., 2000, PhD Thesis, Bangalore university, Bangalore  
Schlichenmaier, R., & Collados, M., 2002, *A&A*, 381, 668  
Walter, D. G., 1978, *Hand Book of Optics*, McGraw-Hill, New York